Hindawi
International Journal of Aerospace Engineering
Volume 2018, Article ID 3252104, 15 pages
https://doi.org/10.1155/2018/3252104

Research Article

Structural Design and Impact Analysis of Deployable Habitat Modules

Yihong Hong[1,2] **Wenjuan Yao**[1] **and Yan Xu**[3]

[1]*Department of Civil Engineering, Shanghai University, Shanghai 200072, China*
[2]*School of Architectural Engineering, Quzhou University, Zhejiang 324000, China*
[3]*School of Aeronautics and Astronautics, Zhejiang University, Hangzhou 310027, China*

Correspondence should be addressed to Wenjuan Yao; wjyao2016@163.com

Received 9 March 2018; Accepted 4 July 2018; Published 4 November 2018

Academic Editor: Christopher J. Damaren

Space-deployable habitat modules provide artificial habitable environments for astronauts and will be widely used for the construction of future space stations and lunar habitats. A novel structural design concept of space-deployable habitat modules consisting of flexible composite shells and deployable trusses has been proposed. Geometric relationships of deployable trusses based on two types of scissor elements were formulated. Flexible composite shells of space habitat modules were designed, and a nonlinear FEA model using ANSYS software was described. Considering folding efficiencies, stiffness, and strength of the structures, the influences of design parameters were analyzed and the final design scheme of space-deployable habitat modules was determined. After detailing the structural designs, low-speed impact dynamic responses between the structures and a stainless steel cylinder were simulated. The analysis results show that dynamic responses are only significant at the point of low-speed impact. The works will provide technical supports for structural designs and engineering applications of space-deployable habitat modules.

1. Introduction

Deployable structure technologies have the advantages of high folding efficiencies, light weights, and low construction costs, which can be used to build future space antennas and lunar habitats [1, 2]. To solve the problems of high launch costs and the difficulties in the construction of rigid space cabins due to their heavy weights and large volumes, there has been extensive research on the structural technologies of space-deployable capsules in the United States and Europe, such as that of NASA's TransHab [3] and the lunar habitats [4]. In May 2016, the Bigelow Expandable Activity Module (BEAM) on the International Space Station was fully expanded, which demonstrates that space-deployable capsule technology can be successfully applied in space missions. Then a series of dynamic tests of BEAM were conducted to assess how the structure responds to impacts that cause vibrations and the structure's ability to dampen the vibrations.

Most recently published research on deployable lunar habitats has been focused on structural system and internal space designs [5], thermal protection system designs [6], structural health monitoring technologies [7], deployment experiments [8], high-speed particle impact tests, etc. The vibration of the space habitat modules occurs during the process of in-orbit expansion, changes of orbit, and attitude adjustments. This vibration is also caused by the influences of in-orbit environments. To date, the dynamic characteristics and dynamic responses of inflatable space modules need to be investigated before these types of structures can be successfully implemented by future space missions [9]. The works researching the dynamics of inflatable structures mostly focused on modal analyses. Liu and He [10] analyzed the dynamic characteristics of inflatable rings in space, considering the material nonlinear characteristics and the influences of design parameters. Apedo et al. [11] investigated the free vibrations of inflatable beams by using the dynamic stiffness method, taking into account large deformation

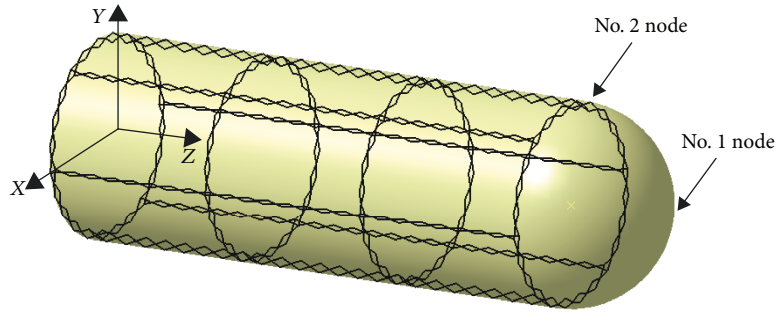

Figure 1: Model of deployable habitat module unit.

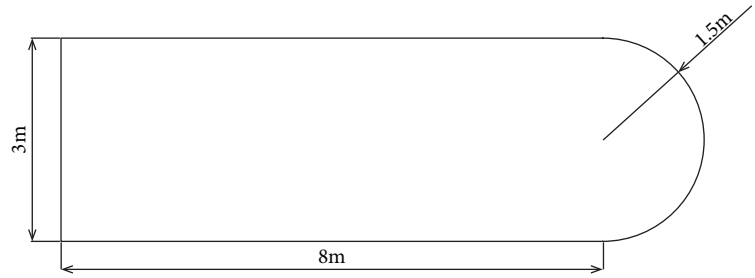

Figure 2: Geometric dimensions of the space habitat modules.

and stress stiffening effects of the applied inflation pressures, and the results were compared with those from a finite-element analysis in ABAQUS software. The dynamic characteristics of space-based inflatable membrane structures were investigated by Zhang et al. [12]. A dimensional analysis was employed to reduce the number of independent variables, and the dimensionless form of the dynamic characteristics was obtained. The natural frequencies and the corresponding modalities of the structures were derived using ANSYS software by Miao et al. [13]. The influences of the structural geometry parameters on the structural vibration modes were studied.

In spite of the above-mentioned research and development efforts, structural designs and transient dynamic responses of space habitat modules still need to be investigated and improved. This paper reports a recently conducted effort that developed an innovative design concept of space-deployable habitat modules consisting of flexible composite shells and deployable trusses. The structural stiffness of the habitat modules is improved, and the design concept is intended for large size habitat modules. The dynamic responses of space-deployable habitat modules need to be investigated carefully, which are helpful for the mechanical performance evaluation and optimization design of the structures. The effect of inflatable prestress was considered in the low-speed impact response analysis.

The remainder of this paper consists of five sections. Section 2 presents the structural designs of space-deployable habitat modules. The deployable trusses based on two types of scissor elements were investigated. A nonlinear FEM analysis model was built using ANSYS software after the flexible composite materials and the load cases were described. Section 3 covers the influence analysis of design parameters on folding volume and mechanical properties. The final design scheme of space-deployable habitat modules was determined. Section 4 describes the low-speed impact dynamic response analysis of space habitat modules caused by the low-speed collisions of a cylindrical colliding object. The dynamic responses of space habitat modules and the cylindrical colliding object during the whole collision process can be obtained. Finally, Section 5 summarizes the concluding remarks and suggestions for future work.

2. Structural Design of Deployable Habitat Modules

2.1. Structural Design Concept. A novel structural design concept of deployable habitat modules is described in this section. The deployable habitat module consists of several habitat module units; a deployable habitat module unit is shown in Figure 1. The coordinate systems and key nodes used in the subsequent analysis are also shown.

The thick wall of deployable habitat modules is flexible composite shells, which include a cylindrical shell and a hemisphere shell. To increase the structural rigidity of deployable habitat modules and reduce the stress levels of the restraint and redundant bladder layers, a deployable truss based on scissor elements is added inside the thick wall. As shown in Figure 1, there are 6 planar trusses along the circumferential direction of the space habitat modules and there are 4 planar truss rings along the longitude direction. The geometric size of deployable space habitat modules is shown in Figure 2.

2.2. Deployable Truss Structure. There are two types of planar trusses in the deployable trusses, as shown in Figure 3. The

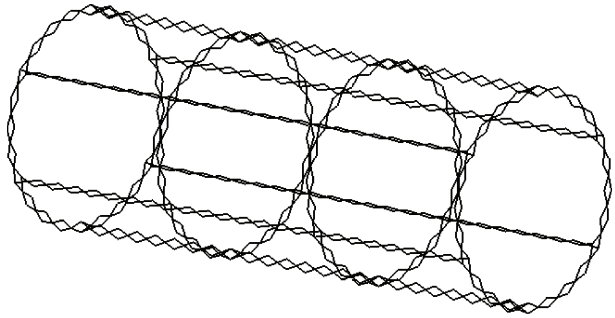

Figure 3: The deployable truss structure.

planar truss ring in the circumferential direction consists of scissor elements with a folding angle, the basic component of which is shown in Figure 4(a). The number of the scissor elements in a planar truss ring is defined as m. The planar truss in the longitude direction consists of scissor elements without a folding angle, the basic component of which is shown in Figure 4(b). The number of the scissor elements in a planar truss is defined as n. There are A planar truss rings in the circumferential direction and B planar trusses in the longitude direction in the whole deployable truss structures. As shown in Figure 3, the values of these parameters are $A = 4$, $B = 6$, and $m = n = 24$.

2.2.1. Scissor Elements with a Folding Angle. The geometric composition of the scissor elements with a folding angle is shown in Figure 5. There are two basic components AED and BEC in the elements, and the folding angle of the basic components is $\angle AED = \angle BEC = \theta$. The relationship formula of the lengths are

$$\begin{aligned} AE &= BE = d_1, \\ ED &= EC = d_2. \end{aligned} \tag{1}$$

The angle between two basic components is $\angle AEB = \beta$, where the value of the angle β is according to the deployable process of deployable trusses. The initial value of the angle is β_0, and the change in angle is defined as $\Delta\beta$. From Figure 5, there are angular relations:

$$\begin{aligned} \angle AEC &= \theta - \beta, \\ \angle BED &= 2\pi - \theta - \beta. \end{aligned} \tag{2}$$

Then the distances of AB and CD can be formulated as

$$AB = 2d_1 \sin\frac{\beta}{2}, \tag{3}$$

$$CD = 2d_2 \sin\frac{\beta}{2}. \tag{4}$$

The local coordinate system of the scissor elements is defined. The origin of the coordinate system is point A and y axis along the line AB. The scissor elements are arranged around the ring, and the extension of lines AB and CD intersect at point O. The corresponding central angle is

$$\alpha = \frac{2\pi}{m}, \tag{5}$$

where m is the number of scissor elements in the deployable truss ring.

The coordinations of each point in the local coordinate system can be obtained: point B is $(0, 2d_1 \sin(\beta/2))$, point E is $(d_1 \cos(\beta/2), d_1 \sin(\beta/2))$, point C is $(d_1 \cos(\beta/2) + d_2 \sin(\theta - \beta/2 - \pi/2), d_1 \sin(\beta/2) - d_2 \cos(\theta - \beta/2 - \pi/2))$, and point D is $(d_1 \cos(\beta/2) + d_2 \cos(\beta/2 + \theta - \pi), d_1 \sin(\beta/2) + d_2 \sin(\beta/2 + \theta - \pi))$.

Then the equation of line OCD is

$$\frac{y_D - y_C}{x_D - x_C} = k = tg\left(\frac{\pi}{2} - \alpha\right). \tag{6}$$

Substitute the coordinates of the points C and D into (6).

$$\frac{d_2 \sin(\beta/2 + \theta - \pi) + d_2 \cos(\theta - \beta/2 - \pi/2)}{d_2 \cos(\beta/2 + \theta - \pi) - d_2 \sin(\theta - \beta/2 - \pi/2)} = tg\left(\frac{\pi}{2} - \alpha\right). \tag{7}$$

The above equation can be simplified to

$$-ctg(\theta) = ctg(\alpha). \tag{8}$$

Finally, the angle formula is obtained:

$$\theta = \pi - \alpha. \tag{9}$$

The equation indicates that when the sum of folding angle α and corresponding central angle θ is equal to 180°, the scissor elements can be arranged around the ring.

The coordinations of point O are

$$\begin{aligned} x_o &= 0, \\ y_o &= y_c - x_c tg\left(\frac{\pi}{2} - \alpha\right). \end{aligned} \tag{10}$$

The outside radius of the planar truss ring is equal to the distance between point O and point B, which is

$$\begin{aligned} R = {} & d_1 \sin\frac{\beta}{2} + d_2 \cos\left(\theta - \frac{\beta}{2} - \frac{\pi}{2}\right) \\ & + \left(d_1 \cos\frac{\beta}{2} + d_2 \sin\left(\theta - \frac{\beta}{2} - \frac{\pi}{2}\right)\right) tg\left(\frac{\pi}{2} - \alpha\right). \end{aligned} \tag{11}$$

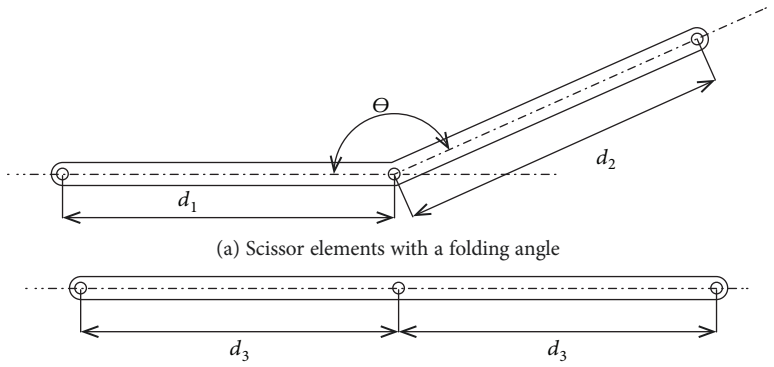

(a) Scissor elements with a folding angle

(b) Scissor elements without a folding angle

Figure 4: Basic component of scissor elements.

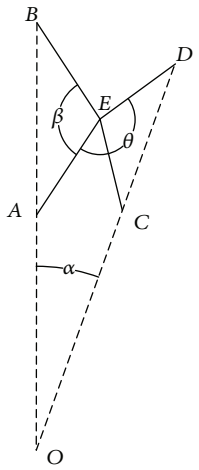

Figure 5: Scissor elements with a folding angle.

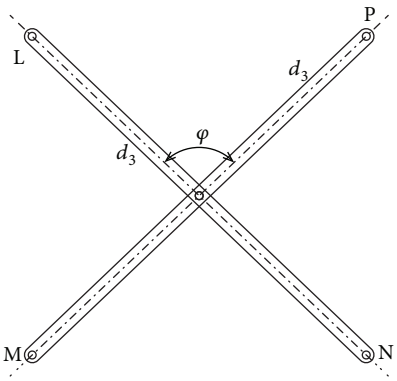

Figure 6: Scissor elements without a folding angle.

If the lengths of two beams in the basic component is designed as $d_1 = d_2$, the outside radius of the planar truss ring is

$$R = d_1\left(\sin\frac{\beta}{2} + \cos\left(\theta - \frac{\beta}{2} - \frac{\pi}{2}\right) + \left(\cos\frac{\beta}{2} + \sin\left(\theta - \frac{\beta}{2} - \frac{\pi}{2}\right)\right) tg\left(\frac{\pi}{2} - \alpha\right)\right). \tag{12}$$

2.2.2. Scissor Elements without a Folding Angle. The planar truss in the longitude direction consists of several scissor elements without a folding angle; the geometric composition of this type of scissor elements is shown in Figure 6. There are two basic components LN and NO in the element, and the angle between the two basic components is φ. The length of each basic component is $2d_3$.

Then the distances between LM and NP and LP and MN are

$$LM = NP = 2d_3 \cos\frac{\varphi}{2}, \tag{13}$$

$$LP = MN = 2d_3 \sin\frac{\varphi}{2}. \tag{14}$$

In deployable trusses, the points L and M connect with the points A and B, respectively, in the scissor elements with a folding angle. Then

$$AB = LM. \tag{15}$$

Substitute (3), (4) (13), and (14) into (15), then

$$2d_3 \cos\frac{\varphi}{2} = 2d_1 \sin\frac{\beta}{2}. \tag{16}$$

The height LP of each scissor element is defined as

$$l = \frac{H}{n} = 2d_3 \sin\frac{\varphi}{2}, \tag{17}$$

where H is the height of the whole deployable truss structures. n is the number of scissor elements along the longitude direction.

Then the angle φ and the length d_3 in each basic component of this type of scissor element are obtained:

$$\varphi = 2\arctan\left(\frac{l}{2d_1 \sin(\beta/2)}\right), \quad d_3 = \sqrt{\left(d_1 \sin\frac{\beta}{2}\right)^2 + \frac{l^2}{4}}. \tag{18}$$

Table 1: Flexible composite shell of space-deployable habitat modules.

Functional layer of thin wall (from outer wall to inner wall)	Composite flexible material	Layer numbers	Total thickness (mm)
Thermal protection layer	Al: Kapton laminated film	1	0.45
	Al: Mylar laminated film	20	
	Al: Kapton laminated film	1	
Space debris and meteoroid protection shielding	Nextel fiber	2	1
	Polyurethane foam	1	75
Restraint layer	Kevlar fabric	1	4
Redundant bladder layer	Vectran fiber	1	3.0
Internal layer	Vectran fabric	11	1.5

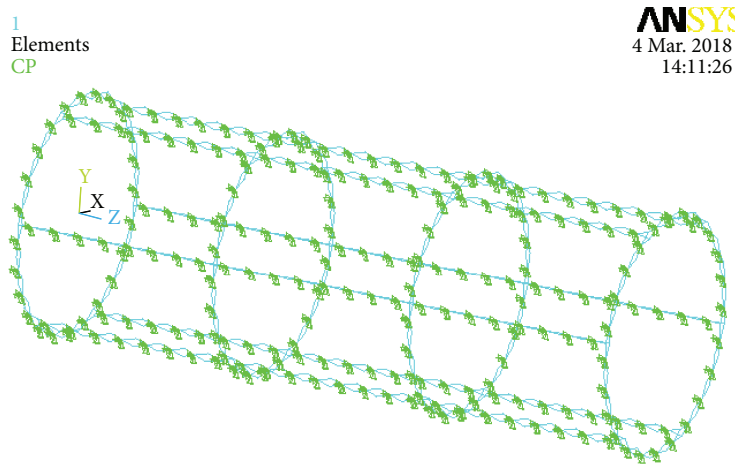

Figure 7: Model of freedom coupling.

2.3. Flexible Composite Shell Design. Space-deployable habitat modules are a type of capsule body structure that consists of flexible composite shells and deployable trusses. Considering the needs of astronauts, space-deployable habitat modules are expanded and pressurized with an internal atmospheric pressurization. As they will be subjected to an internal pressurization load and must serve as an effective radiation and thermal shield, the thin walls of space-deployable habitat modules were designed to be composite membranes consisting of several dozen layers of flexible material. According to their functions, these composite membranes can be divided into a thermal protection layer, space debris and meteoroid protection shielding, a restraint layer, a redundant bladder layer, and an internal layer. Referring to the material design scheme of the TransHab inflatable module [2], the flexible composite shell of space-deployable habitat modules is presented in Table 1 after a design improvement was determined. The total thickness of the composite thick wall is 85 mm.

2.4. FEA Model of Deployable Habitat Modules. A nonlinear finite-element analysis model of space-deployable habitat modules was performed using ANSYS software. Beam188 element is used to model deployable trusses. There are 4 beam elements in a scissor element, and the number of Beam188 elements in the whole structures is $A \times m \times 4 + B \times n \times 4$. The section of Beam188 elements is a ring, of which the outer diameter is 25 mm and the wall thickness is 5 mm. And the material of the deployable trusses is aluminum alloy. The intermediate joints in two types of scissor elements shown in Figures 5 and 6 are ideal hinged joints, and the rotation axis is perpendicular to the plane of the scissor elements. In ANSYS, this rotational freedom is released and the other five degrees of freedom of the joints are coupled with the CP command. The model of freedom coupling in the truss structures is shown in Figure 7.

The SHELL181 element available in ANSYS was used to model flexible composite shells in space-deployable habitat modules, which is shown in Table 1. Both the bending and membrane stiffness capabilities of the SHELL181 element were accounted for in the model. SHELL181 is a 4-node 3D shell element in which each node has six degrees of freedom; the shell can simulate more than 255 layers. Thus, it has been widely used in composite material analysis. It is straightforward to design the layer parameters of the composite material, such as the individual component material, layer sequences, and layer angles, and display them intuitively in the graphics window, as shown in Figure 8.

The connection between deployable trusses and flexible composite shells is realized through the ideal hinged joints

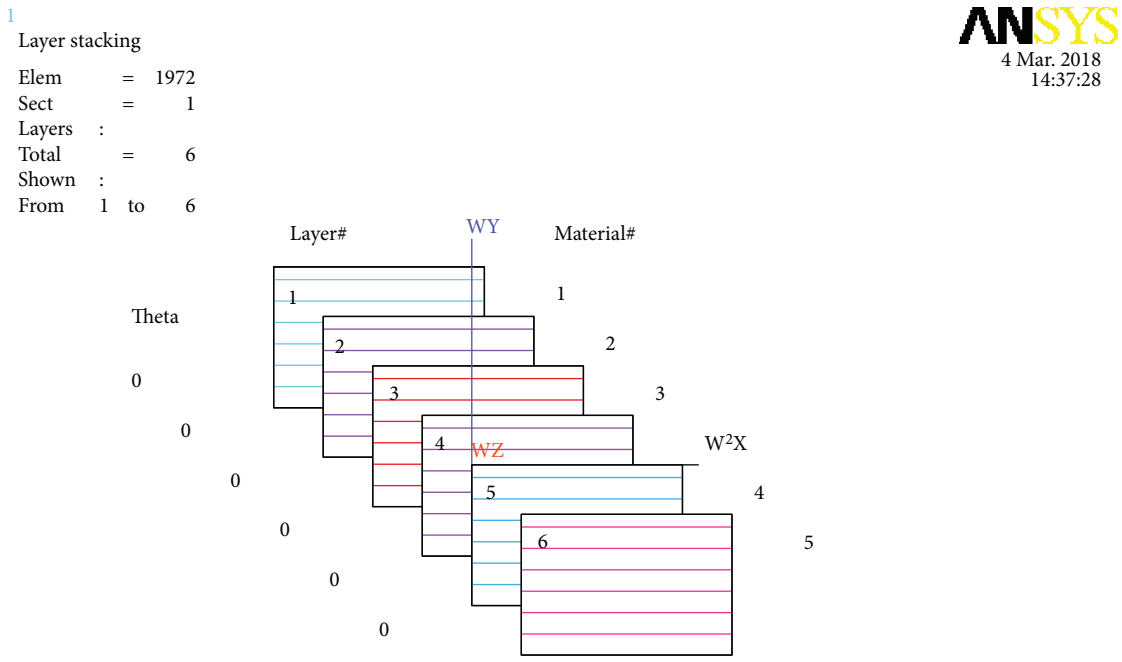

Figure 8: Layer parameters of flexible composite shell.

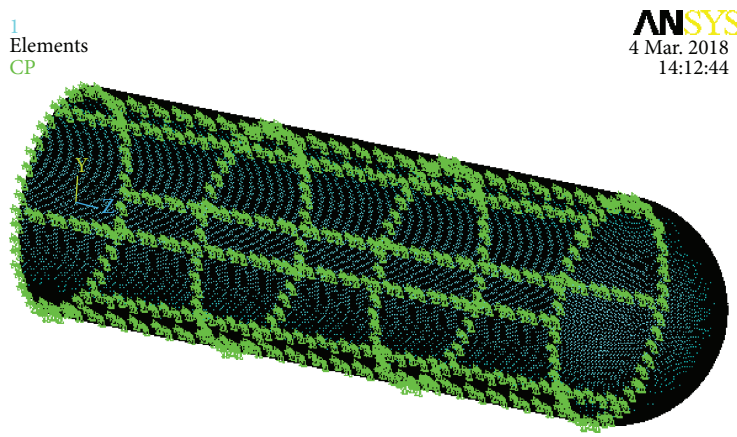

Figure 9: Connection between deployable truss and flexible composite shell.

in which the coordinates of two joints coincide. In ANSYS, three translational degrees of freedom for corresponding two joints are coupled with the CP command in the nodal local coordinate system, as shown in Figure 9.

The left-end section of space-deployable habitat modules is fixed on the spacecraft structures, and the right end is free. The nonlinear finite-element analysis model of space-deployable habitat modules is shown in Figure 10. In the model, the No. 2 node is the node at the y coordinate 1.5 m in the connecting cross section between the cylindrical shell and the spherical shell and the No. 1 node is the vertex node of the inflatable spherical shell on the right end of the structure, as shown in Figure 1. The internal pressurization of space-deployable habitat modules is one atmosphere. Considering the stress rigidization and the geometrical nonlinearity of flexible composite shells, the large deformation (nlgeom, on) and the stress rigidization effect (sstif, on) are opened in the calculation process.

3. Geometry Parameter Analysis and Design

When designing the space-deployable habitat modules, the stiffness and strength of the structures need to be taken into account. Under ensuring structural strength and rigidity, the whole quality and folding volume of the structures must be reduced as far as possible. The structural topology of deployable trusses is determined by geometry parameters A, B, m, n, and β_0, which are defined in Section 2.2. The stiffness, strength, whole quality, and folding volume are also determined by these geometry parameters. The influences of these parameters on folding volume and mechanical properties are investigated in this section.

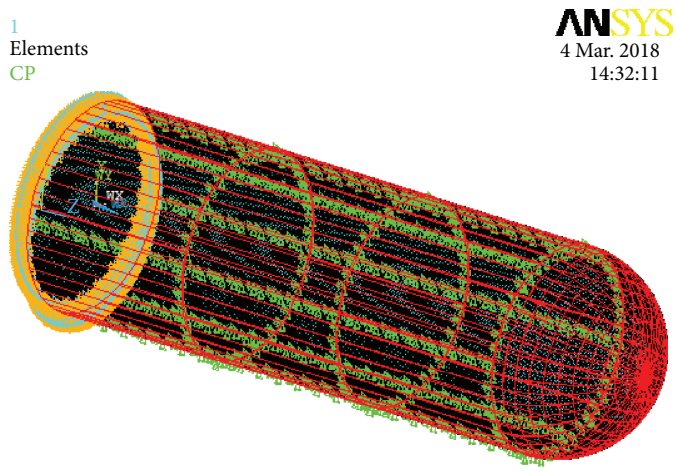

Figure 10: FEM analysis model of the habitat modules.

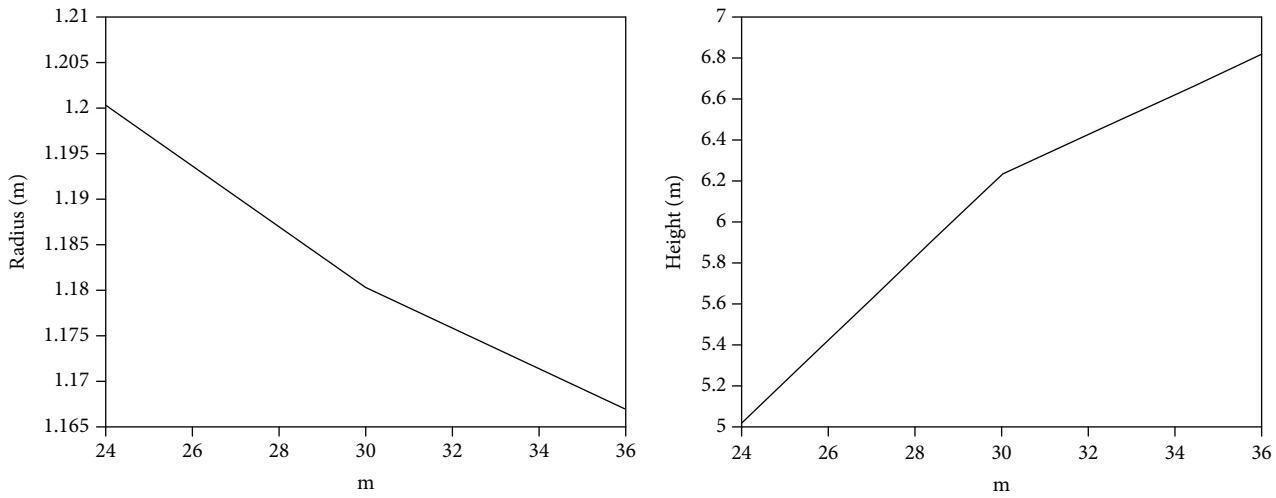

(a) The radius of the folding state

(b) The height of the folding state

Figure 11: Change of the radius and the height of folding state with m.

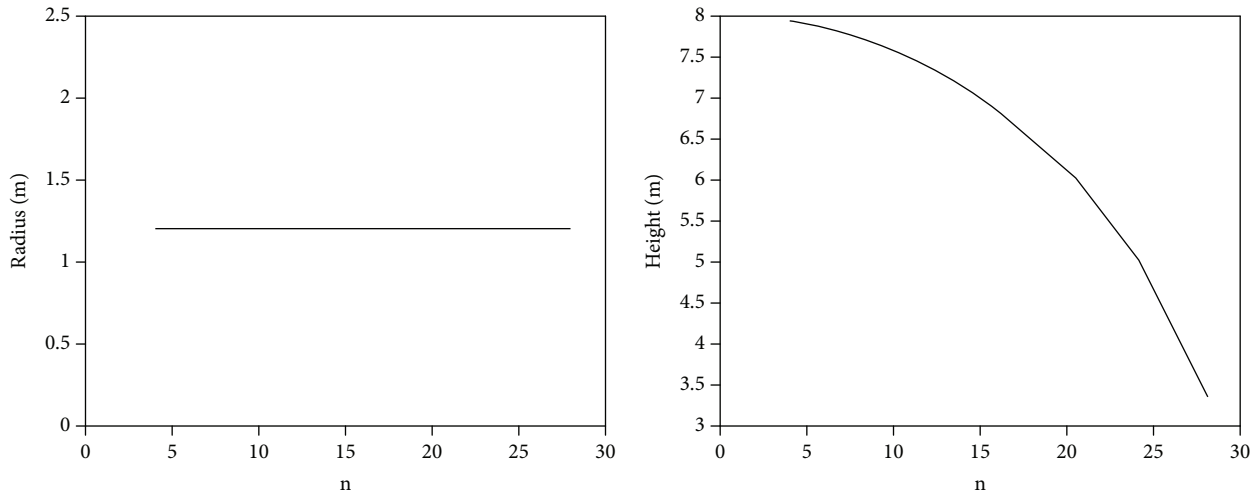

(a) The radius of the folding state

(b) The height of the folding state

Figure 12: Change of the radius and the height of folding state with n.

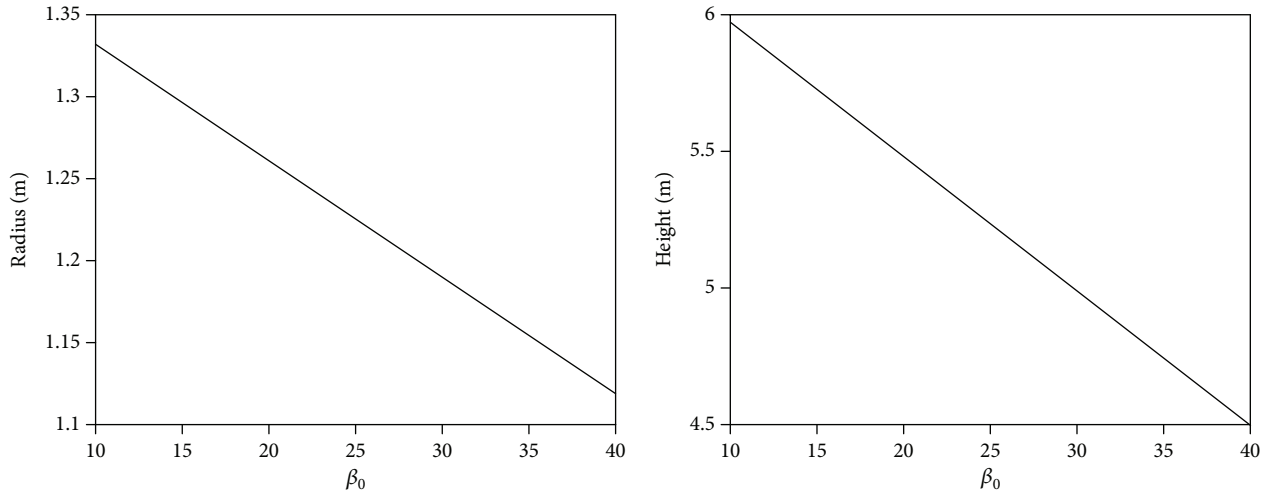

(a) The radius of the folding state (b) The height of the folding state

Figure 13: Relationship curve between the initial values of the angle and the folding states.

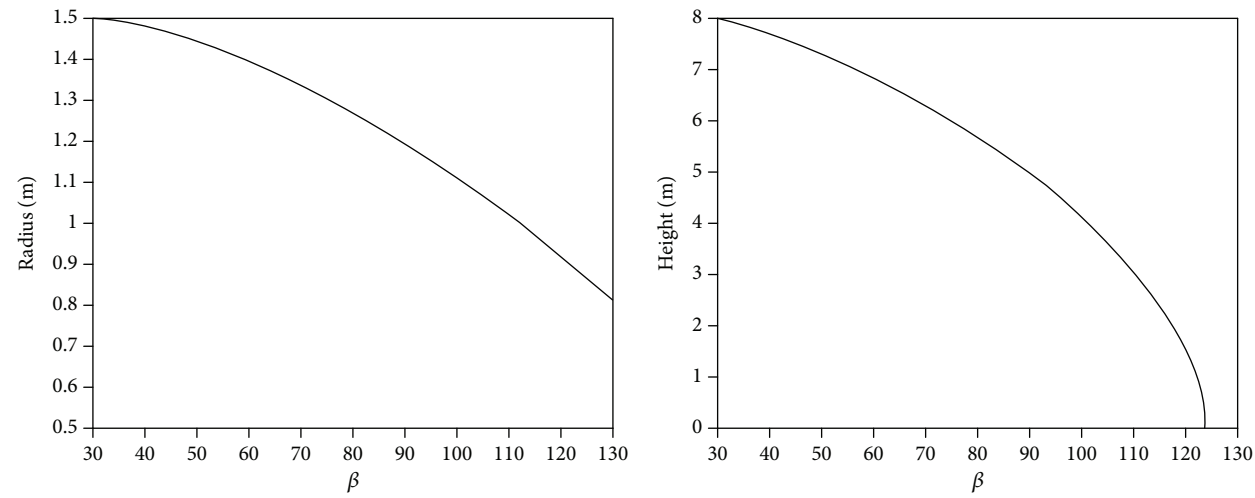

(a) The radius of the folding state (b) The height of the folding state

Figure 14: Relationship curve between the values of the angle and the folding states.

3.1. The Influence on Folding Volume. The initial value of the angle β_0 is designed to be 30° and the change $\Delta\beta$ in the angle is defined to be 60°; n is 24. The value of m is set to be 24, 30, and 36. The change curves of the radius and the height in folding state with m is shown in Figure 11. It can be seen from the analysis results, with the increase of m, the radius of the folding state decreases and the height of the folding state keeps increasing.

The initial value of the angle β_0 is designed to be 30°, and the change in the angle $\Delta\beta$ is defined to be 60°; m is 24. The value of n is set to be 4, 8, 12, 16, 20, 24, and 28. The change curves of the radius and the height in the folding state with n is shown in Figure 12. It can be seen from Figure 12, with the increase of n, that the radius of the folding state is an invariant value and the height of the folding state decreases.

The initial value of the angle β_0 is designed to be different values, and the change $\Delta\beta$ in the angle is defined to be 60°.

Table 2: Average values of each nodal displacement of 9 design schemes.

No.	A, B	UX (m)	UY (m)	UZ (m)
1	$A = 4$, $B = 3$	0.007411	0.007413	0.000316
2	$A = 4$, $B = 4$	0.007282	0.007284	0.000303
3	$A = 4$, $B = 6$	0.007054	0.007055	0.000276
4	$A = 5$, $B = 3$	0.007414	0.007415	0.000317
5	$A = 5$, $B = 4$	0.007283	0.007285	0.000304
6	$A = 5$, $B = 6$	0.007053	0.007054	0.000277
7	$A = 6$, $B = 3$	0.007416	0.007417	0.000318
8	$A = 6$, $B = 4$	0.007282	0.007284	0.000304
9	$A = 6$, $B = 6$	0.007047	0.007047	0.000277

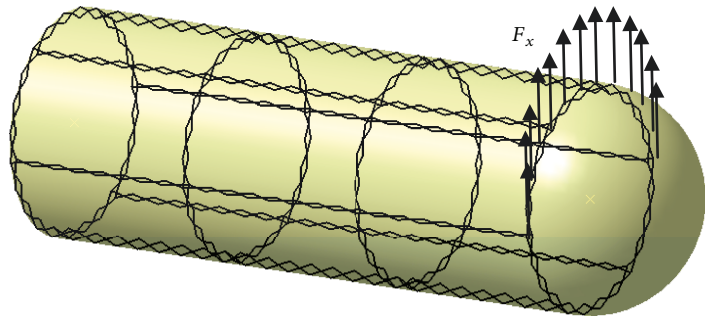

Figure 15: Nodal loads acted at each node.

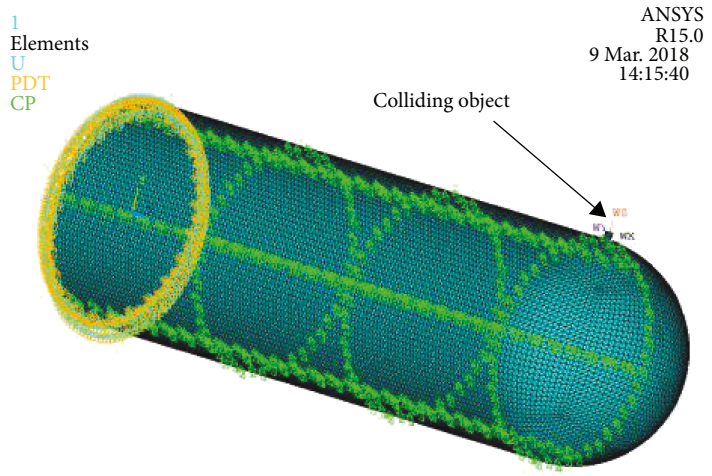

Figure 16: Analysis model of low-speed collision.

The relationship curve between the initial value of the angle β_0 and the radius of the folding state is shown in Figure 13(a)). The relationship curve between the initial value of the angle β_0 and the height of the folding state is shown in Figure 13(b)). It can be seen that the radius and the height of the folding state decreases with the increase of initial value of the angle β_0.

The initial value of the angle β_0 is designed to be 30° and n and m are designed to be 24. When the change on the angle $\Delta\beta$ becomes larger, the deployable trusses and the whole structures will be folded. The relationship curve between the angle between two basic components $\beta = \beta_0 + \Delta\beta$ and the radius of the structure during the folding process is shown in Figure 14(a)). The relationship curve between the angle between two basic components β and the height of the structure during the folding process is shown in Figure 14(b)).

When the value of angle β is 122.5°, the radius of the structure is changed to be 0.9 m and the height is 1.0 m. The folding volume of the whole structures is 2.54 m^3, which is about 4.5% of the structural volume before folding.

3.2. The Influence on Mechanical Properties. The mechanical properties of space-deployable habitat modules mainly include structural strength and stiffness. The number of planar truss rings in the circumferential direction A is designed to be 4, 5, and 7, and the number of planar truss in longitude direction B is designed to be 3, 4, and 6, respectively. Structural strength analysis and structural rigidity analysis of 9 design schemes, as shown in Table 2, were carried out by FEA model of space-deployable habitat modules.

In structural strength analysis, stress analysis of the structures under one atmospheric pressure is performed; the maximum von Mises stress value of the truss beams and each layer of flexible composite shell are evaluated. The maximum stress criterion is applied as the strength criterion. The maximum stresses of the deployable truss members are far less than the strength of aluminum alloy in 9 design schemes. The maximum stresses of thermal protection layer, space debris and meteoroid protection shielding, and internal layer in the flexible composite shell are also less than the strength of aluminum alloy in each design scheme. But the maximum stresses of the restraint layer and redundant bladder layer are close to the tensile strength of the materials. It should be considered carefully in the structural design.

In structural stiffness analysis, static deformations of the whole structures under the nodal loads acted at each node of the $z = 8$ cross section of deployable trusses are analyzed. The nodal loads at each node is $F_x = 10$ kN, $F_y = 10$ kN, and $F_z = 41$ kN in three load cases. One of the three load cases is shown in Figure 15; F_x is on 24 nodes of the

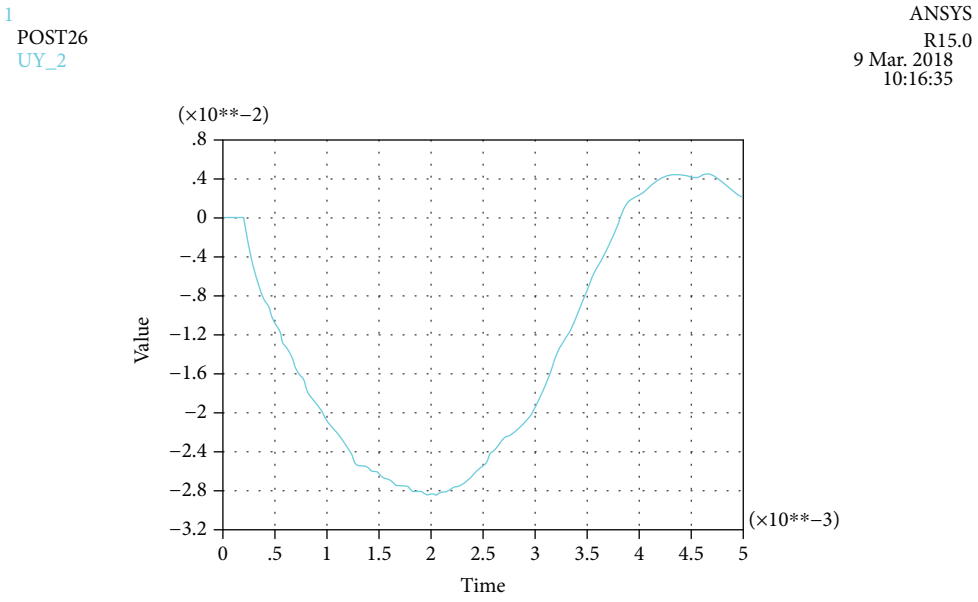

(a) UY displacement response

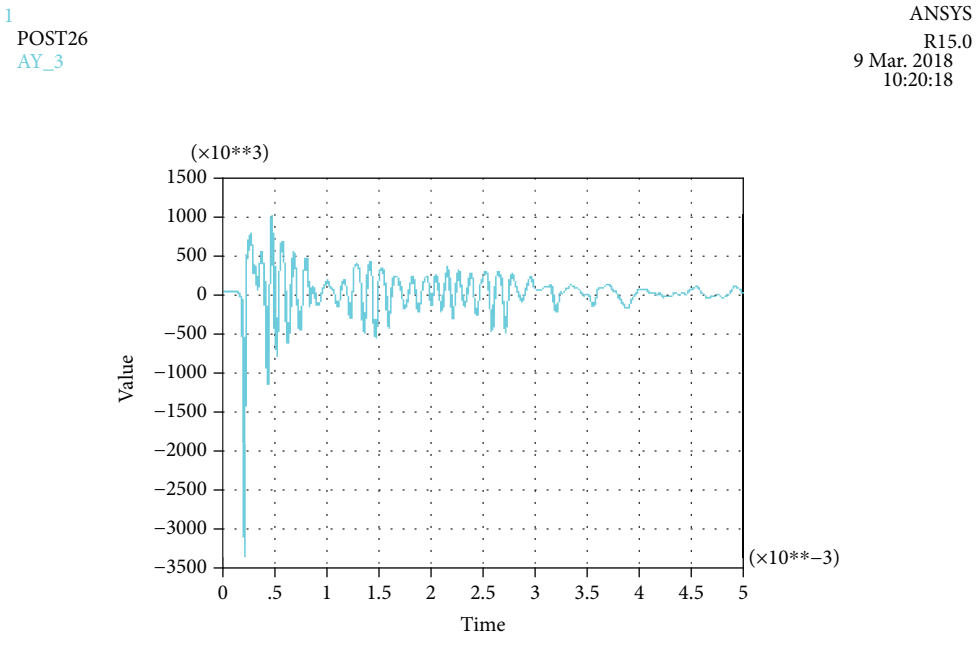

(b) AY acceleration response

Figure 17: Dynamic response of the No. 2 node.

deployable truss ring. The corresponding nodal displacements UX, UY, and UZ of 24 nodes are obtained. Then the average values of each nodal displacement are obtained, which are shown in Table 2.

From the analysis results of the structural stiffness analysis, the structural stiffness of the x direction is basically the same as that in the y direction and less than that in the z direction in 9 design schemes. The number of planar truss rings in the circumferential direction A has little effect on structural stiffness. With the increase of parameter B, the structural stiffness in the three directions increases. With the increase of parameters A and B, the whole quality of the structures increases. So parameter A is designed to be as small as possible and parameter B is designed to be large.

The analysis results of structural strength and stiffness are evaluated comprehensively, and the No. 3 design scheme ($A = 4$, $B = 6$) is selected finally. The deployable truss structures corresponding to the No. 3 design scheme is shown in Figure 3.

4. Low-Speed Impact Dynamic Analysis

The space-deployable habitat modules will inevitably collide with other objects during their service lives, such as the

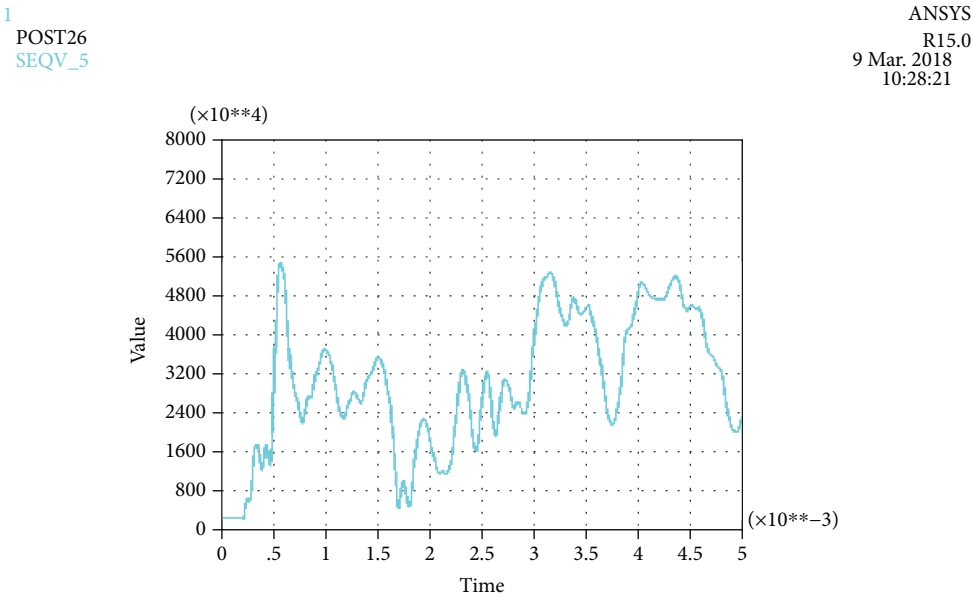

Figure 18: Mises stress response of the No. 1439 element.

astronauts colliding with the thick walls of the habitation modules while walking on board or the space manipulator systems colliding with the thick walls during the unloading of supplies or maintenance. This type of collision is a low-speed impact relative to the impacts of space debris. The purpose of this section is to describe the analysis model and simulation results of low-speed impact.

4.1. Analysis Model of Low-Speed Impact. Analysis model of low-speed impact is shown in Figure 16. The materials and shapes of the actual colliding objects are very complex, so it is assumed that the colliding object is a cylinder with a diameter of 50 mm and a height of 100 mm. The material of the colliding object is stainless steel. In its initial state, the colliding object impacts outside of the No. 2 node. The distance from the colliding object to the outer wall of space-deployable habitat modules is 5 mm. The colliding object moves towards the space habitat module at an initial velocity of 50 m/s.

The analysis type is set to be transient, and the FEA model of the deployable habitat modules has been described in detail in Section 2.4. The effect of inflatable prestress is considered in the low-speed impact response analysis. To analyze the dynamic responses of the habitat modules to the low-speed collisions, the SOLID185 element in the ANSYS software is used to simulate the cylindrical colliding object. The CONTA173 and TARGE170 elements are used to model the contact between the bottom of the cylinder and the outer wall of the space habitat module. The frictional force during the contact and collision process is not considered in the analysis model. To reduce the computational cost, the adaptive time step technology used in the solution is adopted. The collision response analysis process is divided into four steps: the inflating process, before the collision, during the collision, and after the collision. The time integral does not begin during the loading step of the inflating process. Before the collision, a rigid body displacement of the cylindrical colliding object occurs and a large time step is adopted. The time step size used in the solution process was [0.0001, 0.0003] s. During and after the collision, a very small time step is used such that the calculation time step is [0.000001, 0.00001] s. Total analysis time of the whole collision process is 0.005 s.

4.2. Dynamic Responses of the Habitat Modules. In the impact response analysis, the dynamic responses of space-deployable habitat modules and the dynamic parameters of the cylindrical colliding object during the whole collision process can be obtained. The UY displacement and AY acceleration responses of the No. 2 node on space-deployable habitat modules are shown in Figure 17. Before 0.00020 s, the colliding object moves as a rigid body at an initial velocity of 50 m/s, and no contact occurs between the space habitat modules and the cylindrical colliding object. Subsequently, a collision occurs between the two objects, and the elastic deformation of the inflatable space habitat module appears as a low-speed collision. The UY displacement of the No. 2 node reaches a maximum value of 28.27 mm at approximately 0.00197 s. Then, the colliding object moves in the reverse direction, and the UY displacement of the No. 2 node gradually decreases until the colliding object separates itself from the space habitat module. Finally, space-deployable habitat modules are left in a state of free vibrations.

During the whole collision process, the Mises stress response time history curve of the No. 1439 element in the flexible composite shells, which is connected to the No. 2 node, is as shown in Figure 18. Locations of the No. 1 node and No. 2 node are shown in Figure 1. According to the analysis results, the Mises stress of the No. 1439 element at

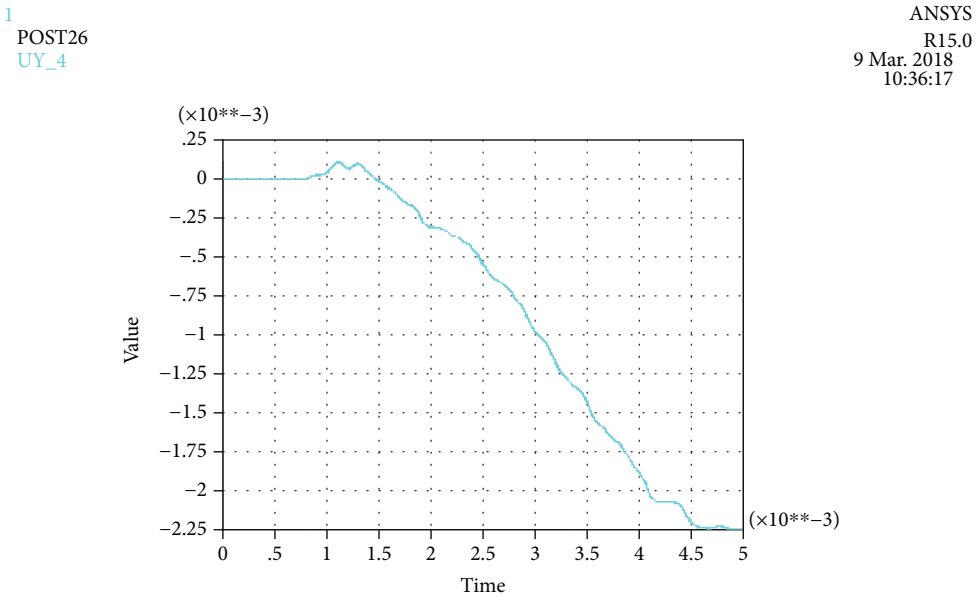

Figure 19: UY displacement response of the No. 1 node.

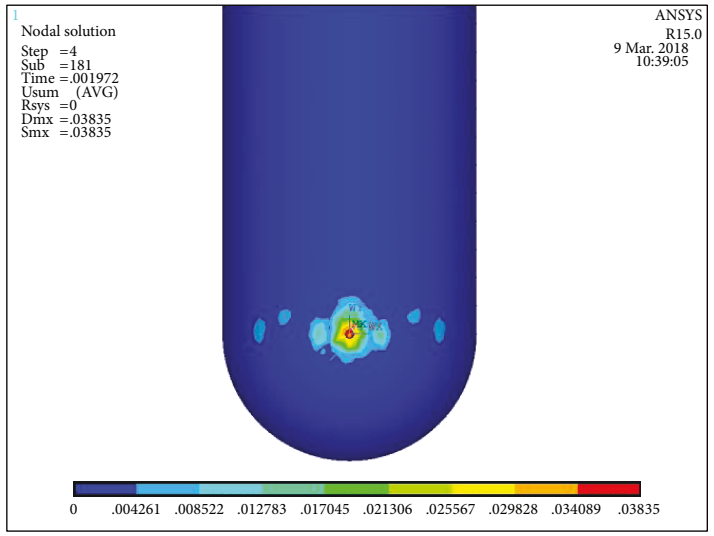

Figure 20: Displacement distribution of the whole structure.

the No. 2 node is approximately 2.94 MPa after the inflating process. The first peak value of the Mises stress is 55.1 MPa at 0.00057 s, and the second peak value at 0.00317 s is 53.08 MPa, which occurs during the collision process. Then, the Mises stress of the No. 1439 element changes at the free vibration stage of the inflatable space habitat module. The peak values of the Mises stress are small compared with the tensile strengths of each layer of composite membranes. During the whole collision process, the flexible composite walls of the space habitat module will not be destroyed.

The UY displacement response time history curve of the No. 1 node is shown in Figure 19. The collision response has not been passed to the node before 0.001 s; thus, the vibration of the No. 1 node is small, such that it is approximately 2.25 mm.

As mentioned above, the largest structural deformation of the habitat modules during the collision process occurs at 0.00197 s. The displacement distribution of the whole structure at this time is shown in Figure 20. It can be seen that the visibly influenced area of low-speed collisions is not large and is mainly confined to a small range on the outer wall below the collision objects.

The colliding object separates itself from the space habitat module fully at 0.00382 s; the displacement distribution of the whole structure at this time is shown in Figure 21. After that moment, the whole space-deployable habitat modules experience free vibration, which diffuses

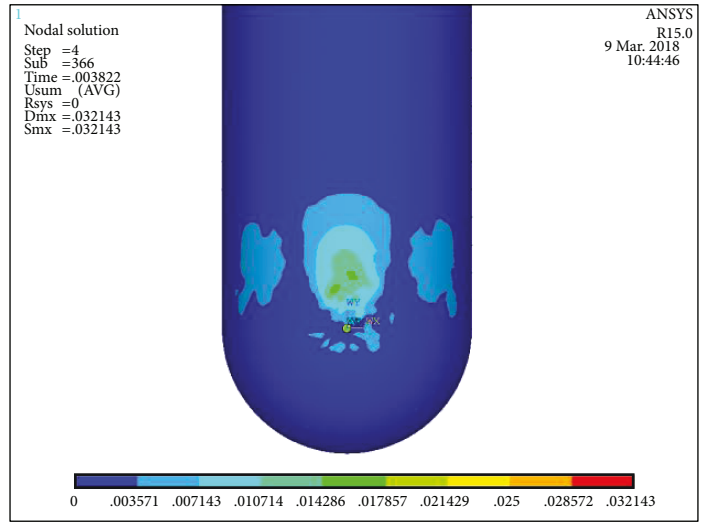

Figure 21: Displacement distribution at time of separation.

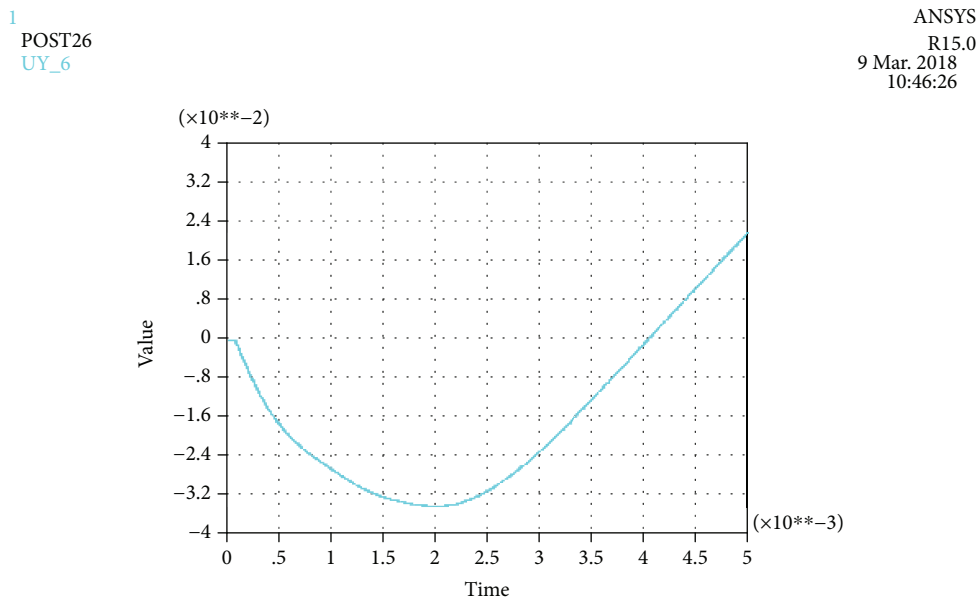

Figure 22: UY displacement response.

along the z-axis. The local elastic deformation caused by the low-speed collision will finally disappear under the action of structural damping.

4.3. Dynamic Responses of the Colliding Object. Then, the dynamic parameters of the colliding object during the low-speed collision are evaluated. The UY displacement response and VY velocity response time history curves of the base center node of the cylinder are shown in Figures 22 and 23. The UY displacement response peak value of the center node at 0.00197 s is about −33.79 mm. The velocity response time history results show that the VY velocity response of the center node at 0.0020 s is −0.19 m/s and the $-Y$ velocity is varied to the $+Y$ velocity after this moment. The VY velocity of the colliding object at the final moment of the collision process is approximately 24 m/s, which is approximately 48% of its velocity before the collision. A part of the kinetic energy of the colliding object is converted into the free vibration energy of the space habitat modules during the low-speed collision process.

5. Conclusion

A novel structural design concept of a space-deployable habitat module consisting of flexible composite shells and deployable trusses has been proposed. The dynamic responses of the space habitat modules under low-speed collision were analyzed. The angle and length relationships of deployable truss based on two types of scissor elements were formulated. When the sum of a folding angle and

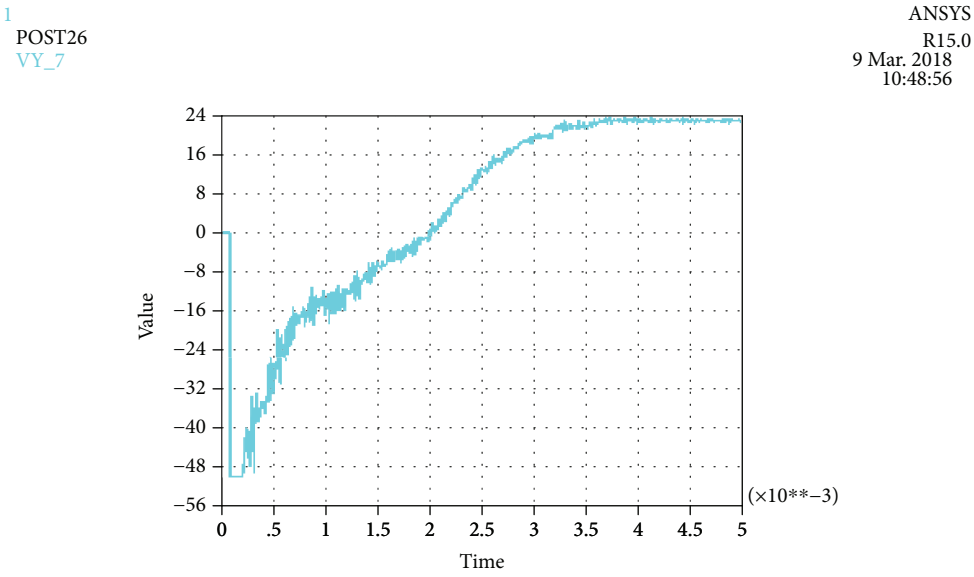

Figure 23: VY velocity response.

corresponding central angle of an element is 180°, the scissor elements with the folding angle can be arranged around the ring. The influence of design parameters on folding volume, stiffness, and strength of the structures was investigated. The geometric parameters m, n, and β_0 mainly affect the folding volume, and the values of these parameters are determined by folding design. The geometric parameters A and B were designed through structural stiffness analysis and structural strength analysis. Then the final design scheme of the deployable habitat modules was determined. Dynamic responses of space-deployable habitat modules under the cylindrical colliding object can be obtained by low-speed collision analysis. The dynamic displacements and stresses are only significant at the point of collision. After the collision process, the colliding object rebounds and a part of the kinetic energy of the colliding object is converted into the free vibration energy of the habitat modules. The current study identifies several questions for future research of this type of space-deployable habitat modules. This study focused on low-speed collisions; thus, hypervelocity collisions of space habitat modules need to be analyzed in future studies [14]. The frictional forces between a colliding object and composite membrane shells need to be considered in future collision analyses.

Data Availability

The data used to support the findings of this study are available from the corresponding author upon request.

Conflicts of Interest

The authors declare that they have no conflicts of interest regarding the publication of this paper.

Acknowledgments

This work was supported by the Quzhou Science and Technology Plan Project (No. 2016y006), the National Natural Science Foundation of China (Grant No. 11402229), and the Zhejiang Province Natural Science Foundation (Grant No. LQ14A020003).

References

[1] Y. Xu and F. L. Guan, "Structure design and mechanical measurement of inflatable antenna," *Acta Astronautica*, vol. 76, no. 1, pp. 13–25, 2012.

[2] Z.-Q. Liu, H. Qiu, X. Li, and S.-L. Yang, "Review of large spacecraft deployable membrane antenna structures," *Chinese Journal of Mechanical Engineering*, vol. 30, no. 6, pp. 1447–1459, 2017.

[3] G. D. Badhwar, H. Huff, R. Wilkins, and S. Thibeault, "Comparison of graphite, aluminum, and TransHab shielding material characteristics in a high-energy neutron field," *Radiation Measurements*, vol. 35, no. 6, pp. 545–549, 2002.

[4] J. Hinkle, A. Dixit, J. Lin, K. Whitley, J. Watson, and G. Valle, "Design development and testing for an expandable lunar habitat," in *AIAA SPACE 2008 Conference & Exposition*, San Diego, CA, USA, September 2008.

[5] D. Y. Yu, Z. J. Ge, and N. D. Wang, "Supposal for structure form of lunar base," *Journal of Astronautics*, vol. 33, no. 12, pp. 1840–1844, 2012.

[6] M. Rais-Rohani, "On structural design of a mobile lunar habitat with multi-layered environmental shielding," Tech. Rep. NASA/CR-2005-213845, 2005.

[7] E. J. Brandon, M. Vozoff, E. A. Kolawa et al., "Structural health management technologies for inflatable/deployable structures: integrating sensing and self-healing," *Acta Astronautica*, vol. 68, no. 7-8, pp. 883–903, 2011.

[8] J. Hinkle, J. Lin, and J. Watson, "Deployment testing of an expandable lunar habitat," in *AIAA SPACE 2009 Conference & Exposition*, pp. 1–9, Pasadena, CA, USA, September 2009.

[9] C. Monticelli, V. Carvelli, Z. Fan, D. Valletti, M. Nebiolo, and A. Messidoro, "Biaxial loading of a textile ribbons structure for an inflatable module of space habitats," *Experimental Techniques*, vol. 41, no. 1, pp. 9–17, 2017.

[10] F. Liu and W. He, "Effect of internal gas on modal analysis of space-inflatable structure," *Journal of Spacecraft and Rockets*, vol. 52, no. 4, pp. 1258–1263, 2015.

[11] K. L. Apedo, S. Ronel, E. Jacquelin, and S. Tiem, "Free vibration analysis of inflatable beam made of orthotropic woven fabric," *Thin-Walled Structures*, vol. 78, pp. 1–15, 2014.

[12] Y. J. Zhang, W. Zhao, and J. Wang, "Analysis of dynamic characteristic of space inflatable membrane structures based on dimensional analysis," *Structure & Environment Engineering*, vol. 43, no. 1, pp. 35–40, 2016.

[13] C. Q. Miao, X. T. Li, and H. Ma, "Modal analysis of support structure of space inflatable antenna," *Journal of Harbin Institute of Technology*, vol. 37, no. 11, pp. 1589–1591, 2005.

[14] R. B. Malla and T. G. Gionet, "Dynamic response of a pressurized frame-membrane lunar structure with regolith cover subjected to impact load," *Journal of Aerospace Engineering*, vol. 26, no. 4, pp. 855–873, 2013.